AEROSPACE REPORT NO.
ATR-88(3728-02)-2

Creep of Carbon Yarns and Composites at High Temperatures

Prepared by

L. A. FELDMAN
Materials Sciences Laboratory

30 September 1988

Laboratory Operations
THE AEROSPACE CORPORATION
El Segundo, CA 90245

Prepared for

OFFICE OF NAVAL RESEARCH
800 North Quincy Street
Arlington, VA 22217

THE AEROSPACE CORPORATION

DISCLAIMER NOTICE

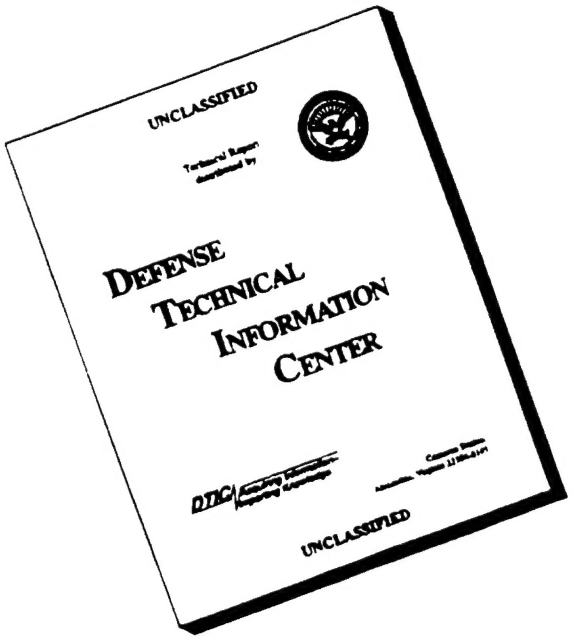

THIS DOCUMENT IS BEST QUALITY AVAILABLE. THE COPY FURNISHED TO DTIC CONTAINED A SIGNIFICANT NUMBER OF PAGES WHICH DO NOT REPRODUCE LEGIBLY.

LABORATORY OPERATIONS

The Aerospace Corporation functions as an "architect-engineer" for national security projects, specializing in advanced military space systems. Providing research support, the corporation's Laboratory Operations conducts experimental and theoretical investigations that focus on the application of scientific and technical advances to such systems. Vital to the success of these investigations is the technical staff's wide-ranging expertise and its ability to stay current with new developments. This expertise is enhanced by a research program aimed at dealing with the many problems associated with rapidly evolving space systems. Contributing their capabilities to the research effort are these individual laboratories:

Aerophysics Laboratory: Launch vehicle and reentry fluid mechanics, heat transfer and flight dynamics; chemical and electric propulsion, propellant chemistry, chemical dynamics, environmental chemistry, trace detection; spacecraft structural mechanics, contamination, thermal and structural control; high temperature thermomechanics, gas kinetics and radiation; cw and pulsed chemical and excimer laser development including chemical kinetics, spectroscopy, optical resonators, beam control, atmospheric propagation, laser effects and countermeasures.

Chemistry and Physics Laboratory: Atmospheric chemical reactions, atmospheric optics, light scattering, state-specific chemical reactions and radiative signatures of missile plumes, sensor out-of-field-of-view rejection, applied laser spectroscopy, laser chemistry, laser optoelectronics, solar cell physics, battery electrochemistry, space vacuum and radiation effects on materials, lubrication and surface phenomena, thermionic emission, photosensitive materials and detectors, atomic frequency standards, and environmental chemistry.

Computer Science Laboratory: Program verification, program translation, performance-sensitive system design, distributed architectures for spaceborne computers, fault-tolerant computer systems, artificial intelligence, microelectronics applications, communication protocols, and computer security.

Electronics Research Laboratory: Microelectronics, solid-state device physics, compound semiconductors, radiation hardening; electro-optics, quantum electronics, solid-state lasers, optical propagation and communications; microwave semiconductor devices, microwave/millimeter wave measurements, diagnostics and radiometry, microwave/millimeter wave thermionic devices; atomic time and frequency standards; antennas, rf systems, electromagnetic propagation phenomena, space communication systems.

Materials Sciences Laboratory: Development of new materials: metals, alloys, ceramics, polymers and their composites, and new forms of carbon; nondestructive evaluation, component failure analysis and reliability; fracture mechanics and stress corrosion; analysis and evaluation of materials at cryogenic and elevated temperatures as well as in space and enemy-induced environments.

Space Sciences Laboratory: Magnetospheric, auroral and cosmic ray physics, wave-particle interactions, magnetospheric plasma waves; atmospheric and ionospheric physics, density and composition of the upper atmosphere, remote sensing using atmospheric radiation; solar physics, infrared astronomy, infrared signature analysis; effects of solar activity, magnetic storms and nuclear explosions on the earth's atmosphere, ionosphere and magnetosphere; effects of electromagnetic and particulate radiations on space systems; space instrumentation.

Report No.
ATR-88(3728-02)-2

CREEP OF CARBON YARNS AND COMPOSITES
AT HIGH TEMPERATURES

Prepared

L. A. Feldman

L. A. Feldman

Approved

Howard A. Katzman

H. A. Katzman, Head
Carbon and Polymers Department

R. W. Fillers, Director
Materials Sciences Laboratory

ABSTRACT

Creep was measured in unidirectional carbon-carbon composites (P55, HM3000, and WCA fibers with A240 and 15V pitch matrices) in tension (2-10 ksi) in the high-temperature range between 2000 and 3000°C. The composites were analyzed by optical and scanning electron microscopy to identify creep-elongation-induced changes in microstructure and mechanical properties. Such changes include matrix microcracking, fiber-matrix debonding, and filament necking. Rate mechanisms were also derived from the measured creep rates. The activation energies for the composites range from 50 to 130 kcal/mole. These values are smaller than activation energies for bulk graphites and indicate low-energy deformation mechanisms. Elastic modulus of the samples was measured before and after creep occurred. The observed increases or decreases are related to specific microstructural changes.

ACKNOWLEDGMENTS

The author thanks Dr. L. H. Peebles of the Office of Naval Research for his continued support of, and interest in, this work. For technical discussions, appreciation is expressed to Drs. R. A. Meyer, D. J. Chang, H. A. Katzman, and G. S. Rellick. The technical assistance of D. C. Robinson and H. G. Hoppe is also acknowledged.

Funding for this effort was processed through SD Contract No. F04701-85-C-0086-P00019 under an Interagency Agreement from the Office of Naval Research.

CONTENTS

FIGURES

TABLES

I. INTRODUCTION

The origin of defects in carbon-carbon (C-C) composites during processing is influenced by the internal stresses developed during successive impregnations and heat treatments. Internal stresses result from chemical decomposition, shrinkage, and thermal expansion mismatch between the higher modulus fibers and the matrix. Porosity and cracks formed during one graphitization cycle may become filled during subsequent impregnation cycles, and further expansion of the material can give rise to the internal stresses (McAllister and Lachman, 1983). At high temperatures, the presence of such stresses may cause damage to the material; however, the stresses may also be relieved through creep, or time-dependent deformation. Creep phenomena are observed in many normally brittle materials at temperatures approaching the melting point.

Studies of the effects of creep of carbon fibers on the processing of C-C composites have been scarce. Early research addressed creep in polycrystalline graphite (Kelly, 1981) and carbon fibers during hot stretching (Hawthorne, 1976). Modeling of the internal-stress-induced failure in C-C composites has taken creep behavior into account mostly theoretically, because of lack of sufficient data for the creep behavior of the fibers and composites (Sines and Cohen, 1982; Chatterjee, 1982).

Previously, we studied creep in unimpregnated carbon yarns and in unidirectional composites to obtain data on high-temperature behavior. The yarns included PAN-based, mesophase-pitch-based, and rayon-based fibers, and matrices were coal tar and petroleum pitches (Feldman, 1987). In the conclusion, we discussed our findings on variations in bonding at the fiber-matrix interface. We indicated that the bonding can be either maintained or decreased after creep, and recommended further studies of the variations. The current work continues that investigation to provide additional information on creep behavior of unidirectional C-C composites and carbon fibers within the composites, such as activation energy, creep

rates, and microstructural effects, at temperatures between 2000 and 3000°C. Such information will enhance understanding of the behavior of the fiber-matrix interface and its influence on creep behavior. Experiments conducted were similar to those detailed in preceding reports; in this most recent work a computer program was incorporated into the system to control sample load and temperature history.

II. EXPERIMENTAL

A. SAMPLE FABRICATION

In referring to carbon and graphite fibers, we generally use the terms filament or single filament to denote individual threads or fiber constituents, which are generally less than about 15 μm in diameter. A fiber tow or yarn refers to a strand or group of filaments, with typically 1,000 to 10,000 filaments per yarn. The term fiber or carbon fiber is often used more generically; for example, when referring to the type of yarn, such as polyacrylonitrile (PAN) based or rayon based.

Several types of carbon fibers and pitch matrix precursors were fabricated into samples and tested; they are listed below.

Fiber/ Modulus	Matrix Precursor
AMOCO WCA (rayon)/5 Msi	Ashland A240 (petroleum pitch)
Hercules HM3000 (PAN)/55 Msi	Allied Chemical 15V (coal tar pitch)
AMOCO P55 (pitch)/55 Msi	

Yarns were impregnated in an apparatus used for forming metal-matrix composite wire (Katzman and Steckel, 1982). Carbon yarn was unwound from a spool and passed over guide wheels, first through a burnoff furnace to heat the yarn to about 400°C in air to remove the sizing, and then through a nitrogen-atmosphere furnace containing a molten mesophase-pitch bath at about 380 to 400°C (see Fig. 1). The mesophase-pitch-impregnated yarn exiting the furnace was then wound onto a large take-up reel.

Samples for creep testing were fabricated by cutting ~20-in. lengths of the impregnated yarn. Loops were formed by gently heating the ends in a stream of hot air to soften the matrix and overlapping the ends (Fig. 1). The 5.1 cm (2-in.)-long overlapped regions were wrapped and tied with

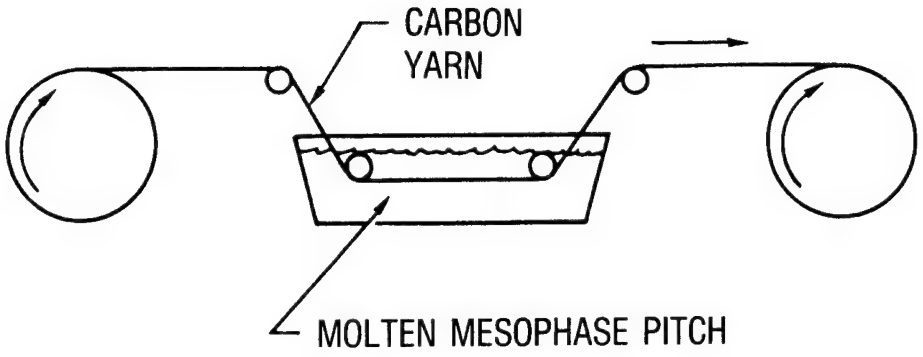

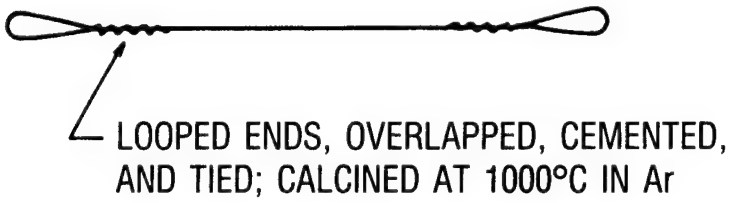

Fig. 1. Schematic of Sample-Preparation Process

cotton thread and a carbonizing cement, leaving a small loop at each end. The looped-end samples were then calcined to 1000°C in argon atmosphere to carbonize the matrix.

B. CREEP MEASUREMENTS

The creep-measurement apparatus is shown in Fig. 2. Samples were gripped at the looped ends and were passed coaxially through a graphite tube furnace under inert-gas atmosphere. Tension, which was applied outside the furnace using an electronically controlled loading device, was monitored at the opposite end of the furnace by a load cell. Temperature was measured with an optical pyrometer and was controlled by an infrared pyrometer. Displacement was measured with a Transtek model 0245-0000 LVDT (linear variable differential transformer). Displacement, load, and temperature data were gathered with a Hewlett-Packard HP85B microcomputer. Additional programs for the HP85B were written or modified to work with the HP3497A data acquisition unit to print and store data and to permit data to be transferred to an HP Integral microcomputer for further analysis.

C. MICROSTRUCTURE

The microstructures of the sample materials were characterized both before and after deformation, using scanning electron microscopy (SEM) and optical microscopy. Microscopy enabled observation of microcracks, and changes in carbon-filament surface morphology, diameter, porosity, and fracture features. Microstructure was examined to aid in relating the observed mechanical properties and behavior of the composites to underlying structures and mechanisms. Bulk density and porosity measurements were also performed, the latter employing the methanol immersion technique. Yarn cross-sectional areas were determined using methanol immersion and lineal density measurements; these areas are required for calculating composite stresses. The area measurements agreed well with the manufacturers' reported or estimated values.

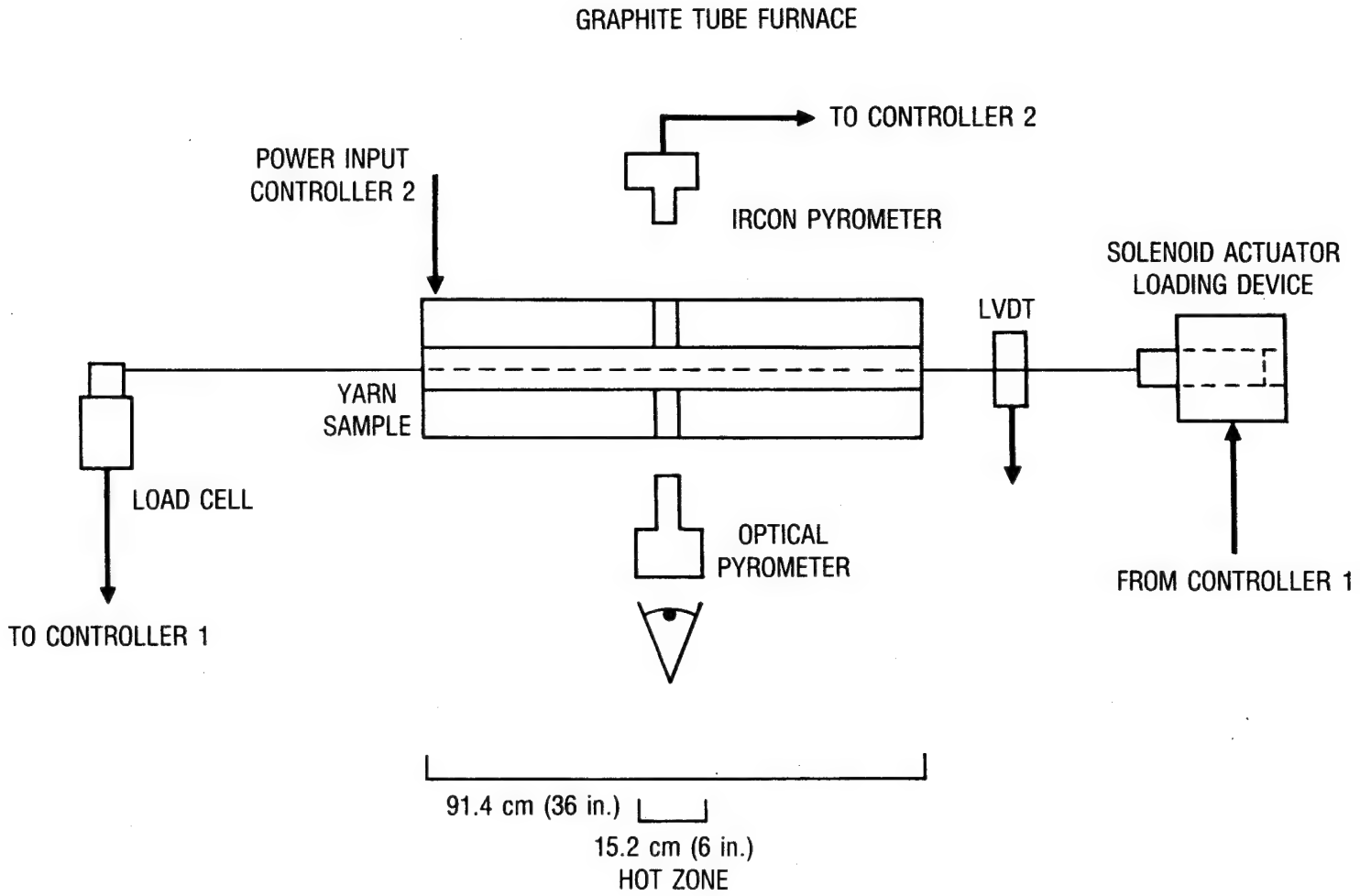

Fig. 2. Schematic of Creep Experiment, Showing Graphite Tube Furnace

D. DYNAMIC MODULUS

Young's modulus of elasticity is defined as "the ratio of tension to extension in a cylinder which is under axial tension and which is unrestricted laterally" (Jaeger, 1971), assuming linear elastic behavior. Measurement of this value, particularly in transverse flexure, can provide information on the efficiency of modulus utilization of the filaments in a unidirectional composite. Modulus utilization efficiency is indicated by the degree to which the theoretical modulus, based on the rule of mixtures (ROM), agrees with the measured value (Feldman, 1985a). Such information can, in turn, give insight into the behavior of fiber-matrix bonding and interaction, changes in fiber or matrix properties, and aspects of composite processing, such as the effects of heat treatment, which can cause utilization efficiency to increase or decrease.

Experimentally, dynamic measurements of elastic modulus were made by vibrating samples transversely: An alternating current was passed through the samples in the presence of a magnetic field. The modulus was calculated from frequency, mass, and dimensions. Density and porosity were characterized by both macroscopic density measurements and the sink-float method (Reynolds, 1968), using methanol (ρ = 0.79 g/cm^3) and 1,2-dibromoethane (ρ = 2.18 g/cm^3). Microstructure was examined by optical and scanning electron microscopy to correlate changes with the modulus measurements. Experimental details are described more completely elsewhere (Feldman, 1983, pp. 3-4; 1985b, pp. 23-30 and 35-62; and 1987, pp. 3-17).

III. RESULTS AND DISCUSSION

A. HIGH-TEMPERATURE CREEP

In the experimental arrangement described here, creep typically became measurable above about 2200°C at stresses in the 14- to 70-MPa (2-10 ksi) range. Thus, our applied stresses are only a few percent of the room-temperature tensile strengths of many types of fibers, which are commonly greater than 2 GPa (300 ksi) (Hughes, 1986). These stresses are much less than those of other recent work on high-temperature creep in unidirectional carbon-carbon composites in which loads about one-third the typical room-temperature tensile strength were used, but at temperatures below 2400°C (Sines et al., 1987).

As a working model, high-temperature creep in the composites was assumed to be thermally activated, as in many high-temperature materials (Kelly, 1981). The activation energy is characteristic of the particular transformation process occurring. Creep studies on pyrolytic graphite in the range 2400-2800°C (Kotlensky, 1966) indicated apparent activation energies of ~250 kcal/mole, which were associated with high-temperature diffusion in graphite by vacancy migration. Other mechanisms at low creep strains (<10-15%) were "dewrinkling" of initially wrinkled graphitic sheet structures, and shear deformation along the basal plane, both of which were related to increases in preferred orientation in the material (Kotlensky, 1965). Results on creep in bulk graphites at temperatures below 2000°C have indicated that enhanced shear processes occur (Green, 1960; Zukas and Green, 1969). It is expected that shear processes will involve lower activation energies, since the basal planes are bound only weakly by Van der Waals forces; the covalent bonds between atoms in the basal planes are much stronger.

Activation energies were calculated from the dependence of the apparent creep rate, dL/dt, on peak hot-zone temperature, T_{max}, given by

$$\frac{1}{L^*}\frac{dL}{dt} = A \exp(-E/kT_{max}) \qquad (1)$$

where L is the sample length, A is a constant, E is the activation energy for creep, and k is Boltzmann's constant. Creep rates were calculated on the basis of "effective" gauge length, L^*, as discussed by Feldman (1985b). Effective gauge length takes into account the fact that creep is occurring over a limited region in the hot zone, a region much smaller than the actual sample length.

Activation energies for WCA/15V and HM3000/15V composites, for example, were 90-130 and 50-70 kcal/mole, respectively; these values are comparable to those obtained earlier for composites with other (nonreinforced) matrices (P55/A240) and for unimpregnated yarns (WCA and P55), which had activation energies in the 60- to 100-kcal/mole range. The relatively low activation energies for both impregnated and unimpregnated yarns indicate that the mechanism for creep is likely to be a consequence of dewrinkling and basal shear rather than the result of a diffusion process. That they are about the same demonstrates that the creep mechanism tends to be governed by the fiber. This result is to be expected, because most of the tensile load is borne by the carbon filaments; the matrix provides mainly interfilament stress transfer.

B. CREEP RATES

Creep rates were calculated using the effective gauge length, L^*, defined by Eq. (1). That length was estimated to be about 15.2 cm (6 in.) in this experiment, as determined by the size of the hot zone and a sample length of about 91.4 cm (36 in.) (Feldman, 1985b). Hot-zone temperatures ranged from 2200 to 3000°C. These conditions resulted in high-temperature creep rates 10 to 20 times smaller than those reported for bulk graphites at similar temperatures and stresses.

Creep rates versus temperature were fit on an Arrhenius plot (logarithmic creep rate versus inverse absolute temperature). A gauge length approximately equal to the hot-zone length of the creep furnace was assumed. Resulting creep rates for various samples were in the range of about 0.1 to 2 × 10^{-6}/sec at 2- to 2.7-ksi tensile stress (referred to yarn cross-sectional area) in the temperature range 2440 to 2740°C (see Table 1). For comparison, creep rates calculated from data for a bulk graphite (Martens et al., 1958) in the same temperature and stress range were between one and two orders of magnitude larger. The data cover a wide range in creep rates. The comparison with bulk graphite is convenient because there is not an extensive amount of creep data available for other forms of carbon.

That the creep rate for unidirectional composites is lower than for other graphitic material is a consequence of two factors: the high alignment of graphitic planes along the fiber axis (Donnet and Bansal, 1984, p. 27), and the loading of the samples under a stress that is an order of magnitude or more smaller than the room-temperature failure strength. Further dewrinkling is also limited by the high degree of alignment already present. For bulk graphite, many Mrozowski microcracks are expected (Kelly, 1981); these are internal cracks caused by the anisotropic thermal shrinkage of graphite crystals on cooling from high temperature. Enhanced local stresses form around these cracks and decrease the strength of bulk graphite relative to that of the composites and lead to enhanced creep. Although microcracks are also found in the composite matrix, they have less effect because most of the load is carried by the filaments.

The ratio of applied stress, $\sigma_{applied}$, to room-temperature tensile strength, σ_{fail}, was much smaller for the composites than for bulk graphite (Table 2). Applied stresses for creep quoted for bulk graphite were ~ 3 ksi. This value is close to the maximum tensile strength at high temperature and is greater than the room-temperature tensile strength of ~ 1.5 ksi. The low relative applied stress in the composites appears to

Table 1. Comparison of Aerospace 1D Data and JPL Data for Creep in Bulk Graphite

JPL Bulk Graphite			Aerospace C-C Composites					
			P55/A240		WCA/A240		P55/15V	
T (°C)	Stress (ksi)	Rate ($\times 10^{-6}$/sec)	Stress (ksi)	Rate ($\times 10^{-6}$/sec)	Stress (ksi)	Rate ($\times 10^{-6}$/sec)	Stress (ksi)	Rate ($\times 10^{-6}$/sec)
2440	2.0	2.5	2.5	0.19	2.7	0.12	2.0	0.067
2500	2.0	4.3	2.5	0.32	2.7	0.21	2.0	0.12
2570	2.0	9.5	2.5	0.55	2.7	0.40	2.0	0.21
2620	2.0	16	2.5	0.86	2.7	0.71	2.0	0.35
2680	2.0	23	2.5	1.4	2.7	1.3	2.0	0.59
2740	2.0	55	2.5	2.1	2.7	2.2	2.0	0.92
E (kcal/mole):		170		110		140		120
A (1/sec):		5.1×10^7		1.12×10^3		1.7×10^5		2.52×10^3

Source of JPL Data: Martens et al. (1958).

Table 2. Ratio of $\sigma_{applied}$ (5 ksi typical) to σ_{fail} (room temperature)

Fiber	σ_{fail} (ksi)	$\sigma_{applied}/\sigma_{fail}$ (%)
P55	300	1.7
WCA	25-50[a]	10-20
HM3000	400	1.3
Bulk graphite	--	90

[a]Minimum based on Union Carbide phenolic laminate data.

contribute to the lower overall creep rates. The lower creep rates can also be associated with the greater length of unbroken reinforcing fiber (of the order of tens of centimeters), contrasted with the typical grain size in bulk graphites (<1 mm).

At low creep elongations, less than a few percent, when most of the filaments are unbroken, the matrix is required to provide less shear stress transfer between filaments and has less chance to influence the creep rates. At higher temperatures and higher elongations, filament breakage and matrix stress transfer become significant. Filament breakage is more marked in unimpregnated yarns, which exhibit final-stage accelerating creep behavior, analogous to tertiary creep in metals. Final-stage accelerating creep is not observed in impregnated composites; instead, filament fracture is localized and appears brittle, as well as fibrous at the fracture surface, but with relatively short pullout lengths (lengths of broken filaments drawn out of the composite and protruding from the broken end), caused by short filament-matrix debonding length (length of filament debonded from the matrix).

Below we discuss some of the microstructural changes accompanying high-temperature creep. Such changes give further understanding of carbon-fiber creep behavior and changes in the fiber-matrix interface.

C. CREEP EFFECTS ON MICROSTRUCTURE AND MODULUS

1. MICROSTRUCTURE

High-temperature creep of the unidirectional composites led to changes in the microstructure. Observed changes included such fracture-zone features as pullouts, filament necking, changes in fiber surface texture, and general matrix microcrack structures associated with either A240 or 15V pitch matrices. These effects are described below.

a. Pullouts

As mentioned above, fracture ends in the high-temperature zone appear to have significant filament pullout; the apparent filament ineffective, or debonded, lengths observed in SEM micrographs vary from a few microns to several centimeters or more at high temperature (Fig. 3). Large pullout lengths in 3D carbon-carbon composites, ranging from 0.3 mm to 3 cm for room-temperature failure, have been discussed by Min and Vinson (1982). Such large lengths are one indication of low fiber-matrix interface strength or poor bonding. The pullout lengths for C-C composites are larger than those typically observed for graphite-epoxy composites, which have better interfacial bonding and strength.

b. Filament Necking

Significant necking of filaments (reduction in filament diameter) occurred at high temperature during creep, indicating high levels of local deformation. Reduction in diameter by a factor of 3 or more was frequently observed. Necking was more extensive in unimpregnated yarn bundles than in impregnated bundles (Fig. 4): An impregnated bundle fractures more abruptly than an unimpregnated bundle, whose fracture occurs filament by filament. This difference indicates the effect of the fiber-matrix interaction: Where the matrix is absent or debonding lengths are large, the loss of stress transfer between filaments causes independent creep deformation of the filaments. When stress transfer through the matrix is present and debonding lengths are shorter, the occurrence of a broken filament in the composite causes the load to be redistributed to other

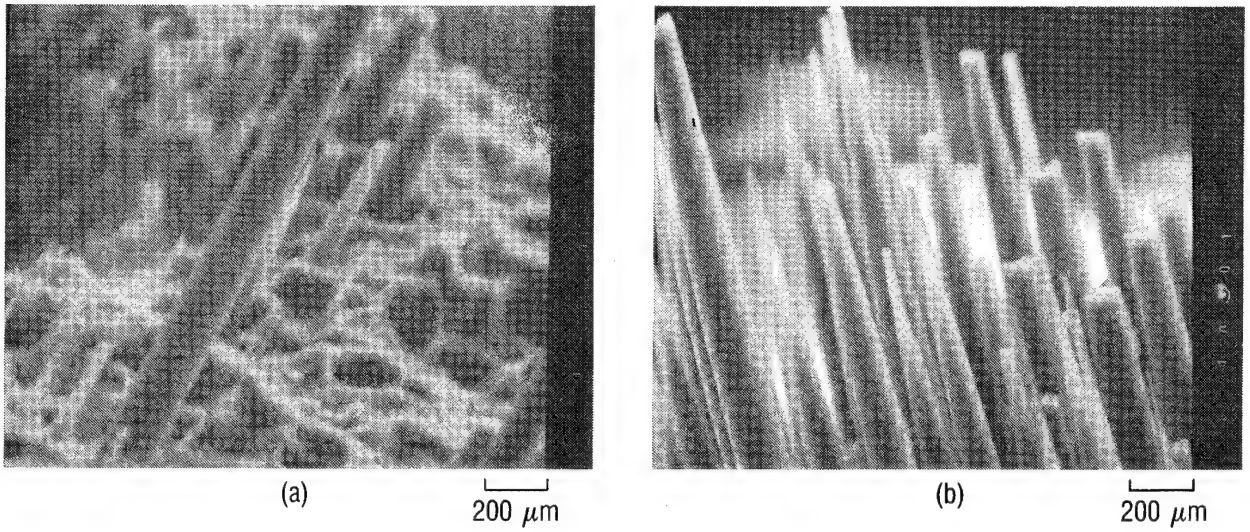

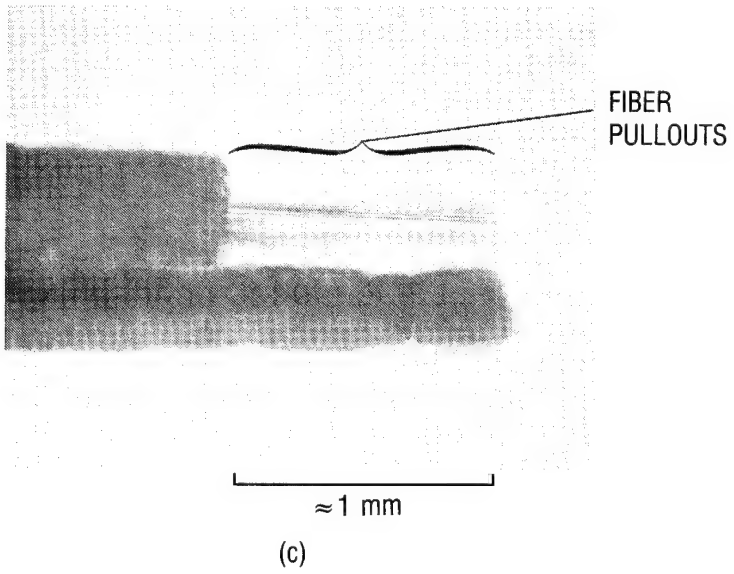

Fig. 3. Optical Micrographs Taken near Fracture Location in P55/15V Composite Sample: (a) pullouts, (b) broken filaments, and (c) low-magnification view of filament pullouts after creep failure at 2750°C.

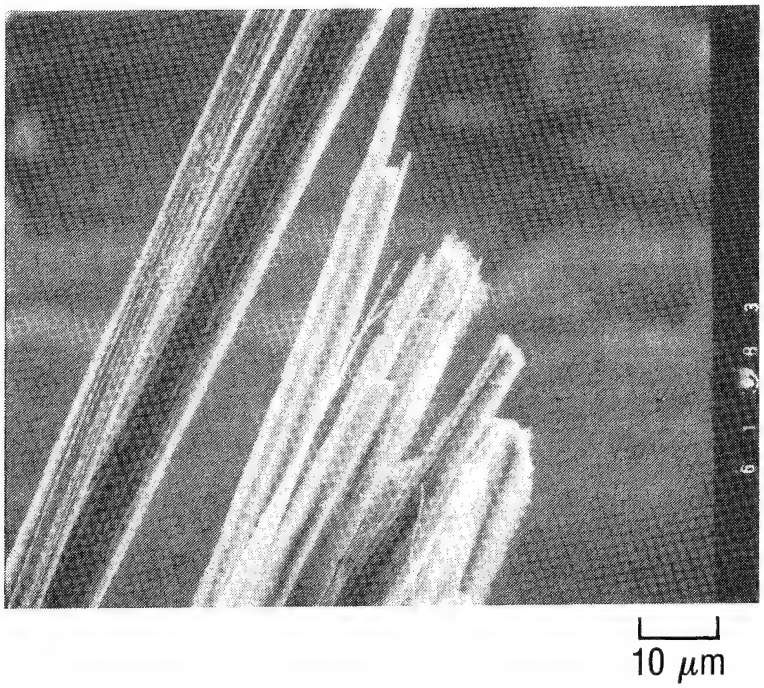

Fig. 4. Filament Necking in Pulled-Out Filaments of P55/15V Composite after Creep Failure at 2800°C

filaments immediately adjacent to the break. Because such stress enhancement is localized, further filament failure is more likely to occur near a previous break, leading in turn to progressively greater localized stress with each successive filament break in the region. The process of enhanced localized stress tends to lead to the localized sample failures observed in these unidirectional composites.

c. Changes in Fiber Surface

Changes in fiber appearance caused by creep deformation included separation into subfilaments, or smaller filaments within the main filament [see Feldman (1983)], and development of fissures and crenulations in the surface, as seen in P55 filaments (Fig. 5). These microstructural features indicate the presence of a substructure within the filaments that may enable deformation and failure to occur inhomogeneously within a filament. This observation for high-temperature creep deformation of filaments agrees with studies on the substructure of various carbon filaments of PAN- or pitch-based origin, in which groups of relatively well-ordered subfilaments or graphitic ribbons within the original filament are revealed by transmission electron microscopy (TEM) (Guigon et al., 1982).

d. Microcrack Structure

A microcrack structure develops in the matrix after many small shrinkage cracks have been introduced. The cracks first appear after the initial pyrolysis and carbonization of the matrix at temperatures around 1000°C, but then grow under the influence of creep in tension at high temperature.

Two types of microcrack structure were noted, appearing in 15V and A240 pitch matrices (Fig. 6). In the 15V matrix, the cracks tended to be larger and coarser, traversing the width of the sample and spaced at fairly regular intervals. The A240 tended to develop a fine crack structure; the cracks were oriented perpendicular to the bundle axis and were randomly dispersed. The reason for the differences between the structures of the two matrices is not clear; variations in total amount of pitch shrinkage,

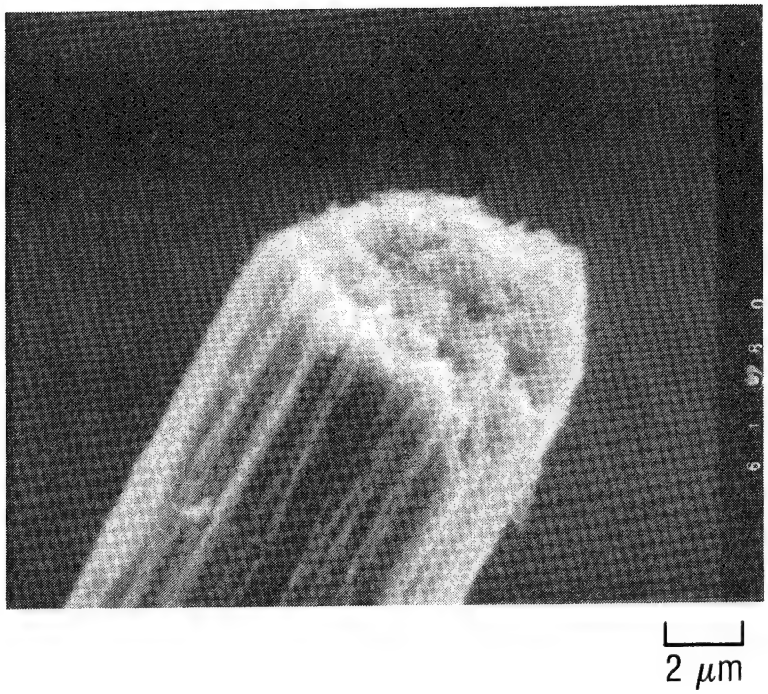

Fig. 5. Fissuring Crenulations after Creep in P55 Filament

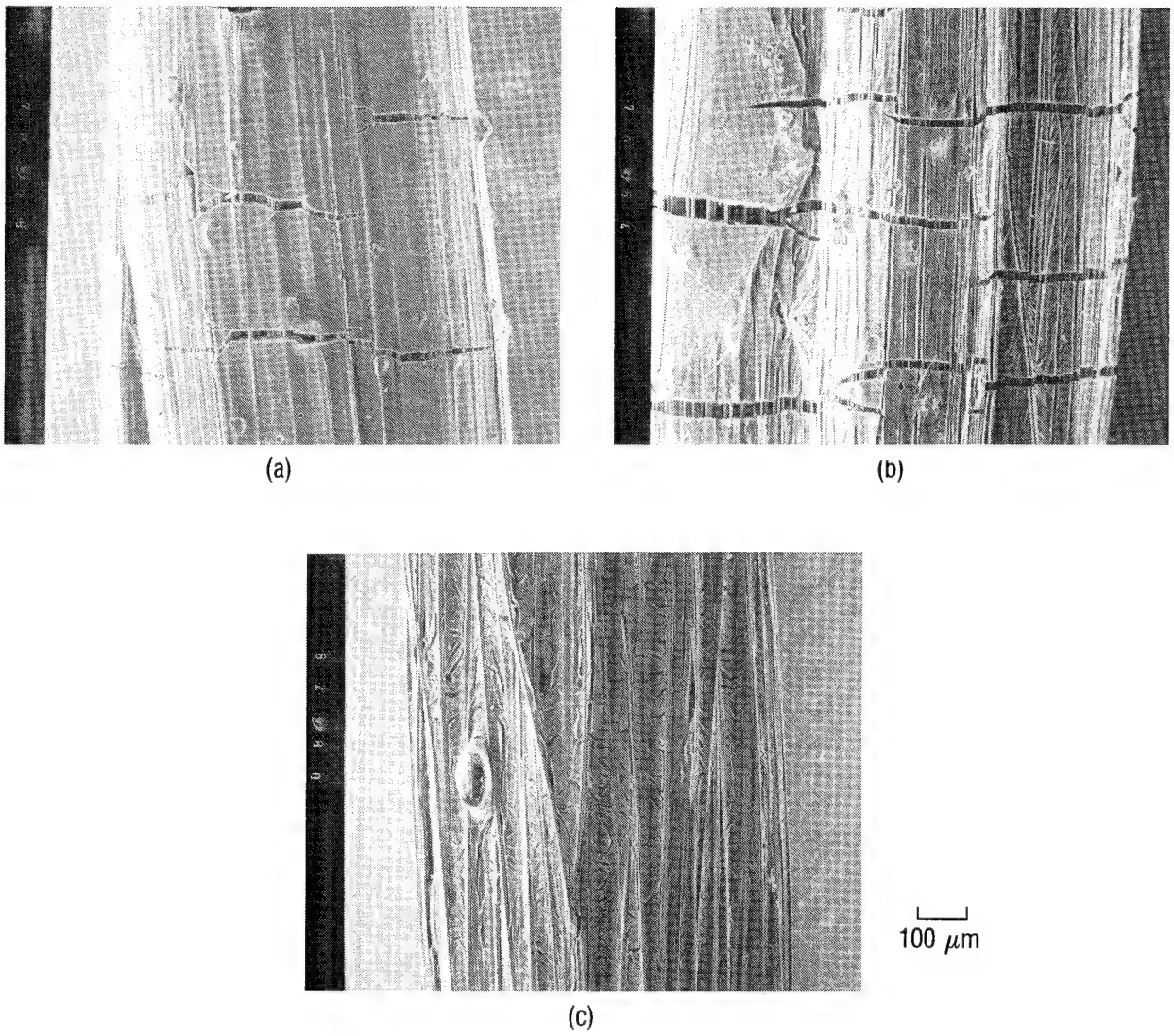

Fig. 6. Differences in Microcrack Morphology Between 15V and A240 Matrices in Two Composites: (a) HM3000/15V composite calcined at 1000°C in argon; (b) HM3000/15V composite after creep at 2750°C; and (c) P55/A240 composite after creep.

and bonding and wetting properties of the pitch in relation to the fiber may explain the differences.

e. Overall Microstructure

Matrix microcracking that exposed the embedded filaments was observed in HM3000/15V and P55/15V composites (see Fig. 7). Scanning electron micrographs at high magnification revealed that, within the microcracks, the diameter of individual filaments was reduced as a result of creep. For both types of fibers, a large reduction in cross section occurs, pointing to large, localized deformation. Filament-to-filament variation in diameter is also evident, which implies that the stress level varies among filaments. Stress-level differences may be attributed to nonuniform fiber-matrix bonding, which causes variations in the amount of the total load that individual filaments experience, and hence the amount of creep deformation they undergo.

2. MODULUS

Modulus measurements can generally be correlated with a number of composite and fiber features, including matrix properties and fiber-matrix bonding. Factors such as changes in composite component properties and changes in the mechanical bonding of the composite can be viewed in terms of modulus translation efficiency, which is expressed as a ratio (or percentage) of the apparent or measured modulus to the calculated rule-of-mixtures values based on known or assumed fiber and matrix elastic properties.

a. Results

P55--Results from P55 fibers with both 15V and A240 matrices indicated that the A240 matrix was more effective in bonding and transferring stress between filaments; that is, it had higher modulus translation efficiency (Table 3). An example of a translation efficiency calculation is given in the Appendix. In fact, there is evidence for a "sheath effect": The modulus calculated for the matrix from the measured composite modulus is much higher than would be expected for an isotropic carbon or graphite. It

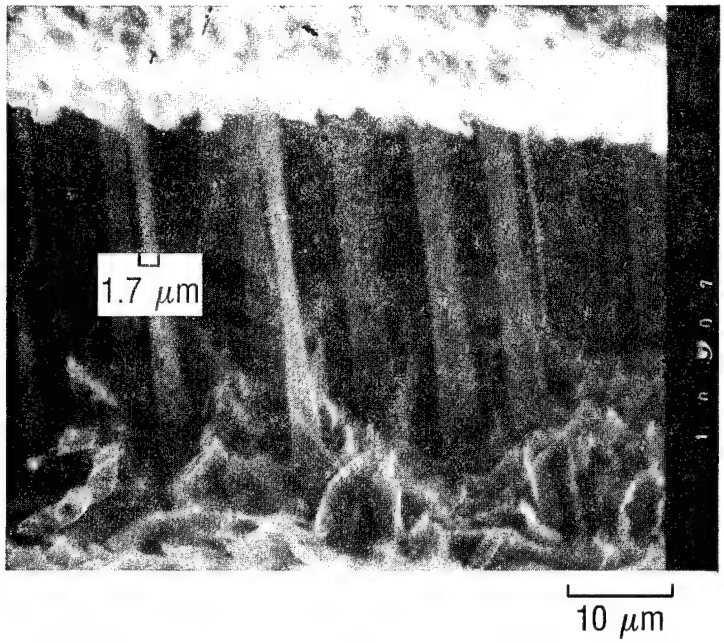

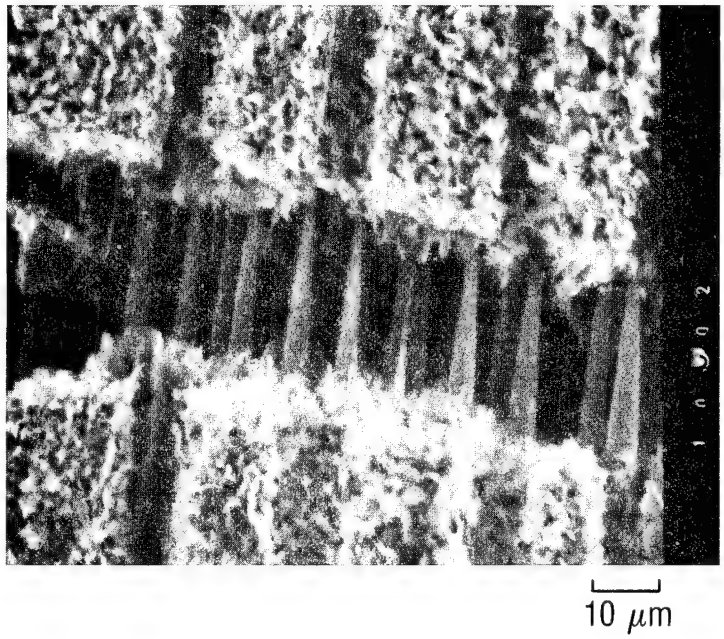

Fig. 7. Two Views of Necking of Filaments within Matrix Microcracks of P55/15V Composite. Original filament diameter = 10 μm.

Table 3. Vibrational Modulus in Impregnated Yarn Samples

	Fiber Diameter D (μm)	Number of Filaments N	Reported Fiber Modulus[a] (Msi)	Composite Modulus E_{meas} (Msi)	ROM Modulus E_{calc} (Msi)	Modulus Translation Efficiency (% ROM)	Density (g/cm^3)
P55/15V	10	2000	55				
As-Impregnated				10.8	18.7	58	1.52
1000°C				17.1	22.4	76	1.23
HM3000/15V	7	3000	50				
As-Impregnated				11.2	31.9	35	1.52
3000°C				1.3	12.0	11	1.38
P55/A240	10	2000	55				
800°C				6.3	11.5	55	1.03
2700°C				22.7	18.1	126	1.26
WCA/A240	9	1440	5[b]				
2700°C				5.7			1.49

[a]Reported by vendor.

[b]Estimated.

suggests a degree of preferred orientation in the matrix. A schematic illustration of the sheath is shown in Fig. 8, in which the graphitic matrix is oriented around the filaments with basal planes parallel to the fiber surface. The effect is a significant contribution of the matrix to the composite modulus: 12 Msi was estimated for the modulus of the sheath (see Appendix). This agrees with quantitative estimates of sheath stiffness (Fitzer and Huttner, 1981; Evangelides et al., 1978). The lower translation efficiency for 15V matrix was interpreted as indicating relatively poor bonding between the 15V matrix and the filaments; poor bonding is supported by observations of longer pullout lengths, variations in the amount of necking of filaments visible within shrinkage cracks, and ability of composites to bend smoothly to a small radius at room temperature with no apparent damage (Feldman, 1985b).

HM3000--Results from this fiber were obtained primarily with a 15V pitch matrix, which, with P55 fibers, formed many large transverse microcracks and did not exhibit good fiber-matrix bonding. The modulus measurements for the HM3000/15V composite indicated lower rule-of-mixtures utilization of fiber modulus than for P55 (11-35%; see Table 3); this is consistent with SEM observations of poorer fiber-matrix bonding in the HM3000/15V composite.

The microstructure seen in the micrographs does not suggest the presence of a sheath; that is, there is little evidence for alignment or striation in the matrix along the filaments. However, a sheath might still have been formed during the early processing stages (pyrolysis and carbonization) and later might have debonded from the filaments during the creep stage. A weak fiber-matrix bond combined with a highly aligned sheath would reduce mechanical properties such as bending stiffness (Greszczuk, 1968). If the sheath effect were present it would not necessarily be evident from studying the mechanical properties.

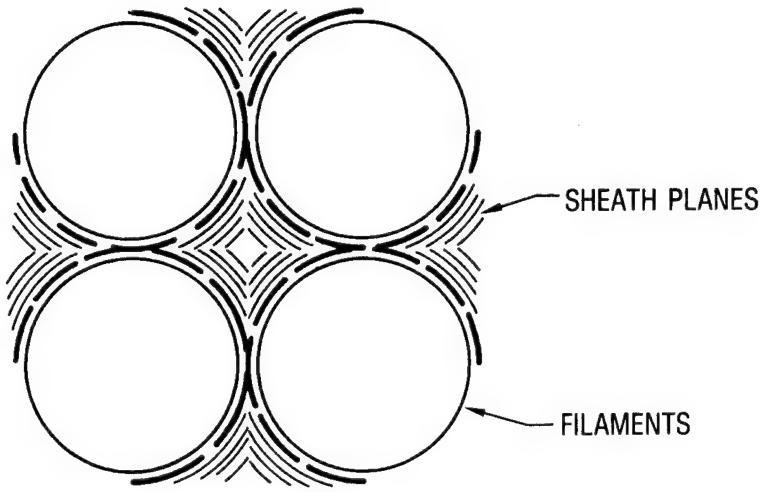

Fig. 8. Sketch of Idealized Sheath Structure (Evangelides et al., 1978)

b. Discussion

Dynamic modulus was calculated from measurements of the frequency of a small beam. The theoretical modulus and frequency of a bundle can be calculated simply, using the rule of mixtures for a unidirectional composite and assuming the matrix makes a negligible contribution to the modulus because its modulus is so much smaller than that of the fiber.

The measured vibrational frequencies of impregnated fiber bundles often disagreed with the theoretical frequencies; there were positive and negative deviations. At least three mechanisms could account for the deviations from expected behavior: the sheath effect (Evangelides et al., 1978; Fitzer and Huttner, 1981); fiber-matrix debonding; and structural changes in the filaments, e.g., induced preferred orientation through heating and stretching, crystallite growth, and degradation of fibers (Donnet and Bansal, 1984).

The first mechanism, production of a sheath effect, may occur for P55/A240 composites. For one sample the measured modulus was greater than 100% of the predicted ROM modulus, based on the assumptions that the filaments were totally responsible for the composite modulus, and the fiber properties were unchanged due to processing. By including the matrix modulus contribution to the composite, it was found that the matrix required an effective modulus of approximately 12 Msi. This value suggests that the matrix was preferentially aligned along the composite axis, which is the sheath effect. This alignment originates from the matrix precursor during the early stages of graphite formation, when the pitch passes through the mesophase regime (White, 1977). The effect tends to extend only a limited distance outward from the fiber surface, of the order of 10 μm or less, so that the sheath around the fiber consists of matrix material with high preferred orientation. Sheath development in the composite matrix is determined by the fiber volume fraction and inter-filament spacing (Zimmer and Wietz, 1985).

Decreased modulus was exhibited for HM3000/15V composites, which appear to have substantial debonding between filaments and matrix. The debonding is depicted in the micrographs in Fig. 7. Necking observable within the microcracks reveals variations in fiber diameters, attributed to different degrees of fiber-matrix bonding. A sufficiently debonded composite may behave in bending as if the fibers act independently, resulting in a very low effective modulus for the composite as measured in bending (Greszczuk, 1968). The low ROM value in HM3000/15V after creep (11%) compared with its higher value after impregnation and before creep (~35%) suggests that fiber-matrix debonding has been introduced during high-temperature creep. The possibility that other factors, such as changes in fiber properties during heat treatment and creep, contribute to the observed changes in the composite, has not been addressed in detail. However, previous x-ray comparisons of filaments undergoing creep versus filaments undergoing heat treatment evidenced that creep itself did not appear to produce changes in the crystallinity or orientation (Feldman, 1983). In other systems, changes in in situ fiber strength in a composite may be caused by high-temperature processing (Leong and Zimmer, 1987).

IV. CONCLUSIONS

Measurements of creep of unidirectional carbon fiber composites at high temperatures indicate that creep rates are, in general, lower than those of bulk graphites under similar conditions. During creep, fiber-matrix debonding occurs and produces several effects, including localized necking of filaments and decrease in flexural modulus as measured by vibrational techniques.

Creep rates for unidirectional composites at high temperatures appear to be thermally activated, although activation energies are somewhat low when compared with those reported on bulk graphites. The low energies imply a different creep mechanism in fibers and composites. The difference may be that vacancy diffusion is the likely rate-governing factor for bulk graphites, whereas, in composites, creep behavior is determined mostly by the fiber properties and to a lesser degree by the fiber-matrix interaction. Unidirectional composites also exhibit lower absolute creep rates at comparable temperatures and loads. The main conclusions are as follows:

- In HM3000/15V and P55/15V composites, extensive fiber-matrix debonding occurs as a result of high-temperature creep.
- The fiber-matrix bonding in the P55/A240 composite remains intact.
- The matrix contributes significantly to the composite stiffness if it is aligned and well bonded (sheath effect).
- The presence of the matrix provides interfilament stress transfer. Compared with unimpregnated yarn, impregnated materials
  - Have lower creep rates;
  - Undergo final failure at higher temperatures; and
  - Exhibit failure as localized fracture rather than filament by filament at different locations.
- Creep-induced debonding can affect the final failure morphology, causing large pullout lengths.

- Activation energies of 50 to 130 kcal/mole for creep are lower than the ≥250 kcal/mole typical for vacancy self-diffusion in graphite. They suggest lower energy processes, such as basal plane slippage and dewrinkling.

- Tensile stresses applied were lower than the room-temperature tensile strength. At these loadings, creep became measurable above about 2200°C.

- Vibrational stiffness measurements indicated composite moduli in the range of 1 to 20 Msi. Generally, lower-than-ROM stiffness was found in the composites after creep. Low stiffness results from extensive matrix microcracking, crack growth, and debonding.

- In composites such as HM3000/15V, deforming at high temperature results in severe necking of unbonded filaments within cracks.

Microstructural observations and modulus measurements indicate the importance of matrix structure and fiber-matrix bonding in determining the mechanical properties of the composite. This information will be of value in determining the effects of creep and high-temperature deformation in the processing of carbon-carbon composites.

V. RECOMMENDATIONS FOR FUTURE WORK

Further work is required to assess the relation of thermal expansion effects to creep, and to separate the thermal expansion contributions from total elongation. Mechanisms for creep at high temperature should also be examined further; for example, by studying preferred orientation changes in detail using techniques such as TEM and x-ray diffraction.

Future work should include testing of other composites; for example, composites using higher-modulus mesophase-pitch fibers, such as P100, and/or non-mesophase-forming matrices, such as phenolics or high-char-yielding material. Such investigations should also include varying the number of impregnation cycles to increase composite density, reduce porosity, and increase fiber-matrix bonding; varying the heat treatment prior to creep to aid in distinguishing effects of graphitization and thermally induced structural changes from creep-induced changes; and changing other factors that may contribute to understanding specific creep mechanisms.

REFERENCES

Chatterjee, S. N., "Effects of Matrix Viscoelasticity and Cracking on Fiber Composite Response During Thermal Cycling," Proceedings of ASME Meeting on Thermomechanical Behavior of High-Temperature Composites, ed. J. Jortner, pp. 51-62 (held in Phoenix, AZ, 14 November 1982).

Donnet, J. B. and R. C. Bansal, Carbon Fibers (Marcel Dekker, New York, 1984).

Evangelides, J. S., et al., Strategic Missiles Materials Technology (SMMT) Program Carbon Materials Analyses, TOR-0078(3726-01)-3, The Aerospace Corporation (10 January 1978).

Feldman, L. A., High-Temperature Creep of Carbon Yarns, First Annual Report, TOR-0083(3728-02)-2, The Aerospace Corporation (5 September 1983).

————, "High Temperature Creep Effects in Carbon Yarns and Composites," Extended Abstracts, 17th Biennial Conference on Carbon, pp. 393-394 (held at Univ. of Kentucky, Lexington, 16-21 June 1985a).

————, High-Temperature Creep of Carbon Yarns, Second Annual Report, TOR-0084A(5728-02)-2, The Aerospace Corporation (15 July 1985b).

————, High-Temperature Creep of Carbon Yarns and Composites, TOR-0086(6728-02)-2, The Aerospace Corporation (30 September 1987).

Fitzer, E. and W. Huttner, "Structure and Strength of Carbon/Carbon Composites" (review), J. Phys. D 14, 347-371 (1981).

Green, L., "High Temperature Creep in Graphite," Proceeding of the 4th Carbon Conference (1960), pp. 497-509.

Greszczuk, L. B., "Theoretical Studies of the Mechanics of the Fiber-Matrix Interface in Composites," in Interfaces in Composites, ASTM Spec. Tech. Publ. (1968), pp. 42-58.

Guigon, M., et al., "Microstructure (Microtexture), Structure and Surface Studies of Some Carbon Fibers," in Progress in Science and Engineering of Composites, eds. T. Hayashi, K. Kawata, and S. Umekawa (ICCM-4, Tokyo, 1982), pp. 91-96.

Hawthorne, H. M., "The Mechanics of Stretch-Graphitization of Glassy Carbon Fibers," J. Mater. Sci. 11, 97-110 (1976).

Hughes, J. D. H., Carbon 24, 551-556 (1986).

Jaeger, J. C., Elasticity, Fracture and Flow (Methuen, London, 1971), p. 57.

Katzman, H. A., and G. L. Steckel, Transverse Strength Properties of Graphite-Aluminum Composites, TOR-0083(3726-01)-1, The Aerospace Corporation (10 October 1982).

Kelly, B. T., Physics of Graphite (Applied Science Publishers, London, 1981).

Kotlensky, W. V., Trans. Metall. Soc. AIME 233, 830-832 (1965).

————, Carbon 4, 209-214 (1966).

Leong, K. and J. Zimmer, 18th Biennial Carbon Conference (American Carbon Society, 1987), pp. 22-23 (held at Worcester Polytechnic Institute, Worcester, MA, 19-24 July 1987).

Martens, H. E., L. D. Jaffee, and D. D. Button, "High-Temperature Short-Time Creep of Graphite," JPL External Publ. 583 (13 November 1958).

McAllister, L. E. and W. L. Lachman, "Multidirectional Carbon-Carbon Composites," Handbook of Composites, Vol. 4, Fabrication of Composites, eds. A. Kelly and S. Mileiko (Elsevier, New York, 1983), Ch. 3.

Min, B. K. and J. A. Vinson, "Nonlinear Behavior and Failure Mechanisms of Three-Dimensional Carbon-Carbon Composites," Proceedings of ASME Meeting on Thermomechanical Behavior of High-Temperature Composites, ed. J. Jortner, pp. 77-90 (held in Phoenix, AZ, 14 November 1982).

Reynolds, W. N., Physical Properties of Graphite (Elsevier, New York, 1968).

Sines, G. and B. J. Cohen, "Stresses During Fabrication of Cylindrically Woven Carbon-Carbon Composites," Proceedings of ASME Meeting on Thermomechanical Behavior of High-Temperature Composites, ed. J. Jortner, pp. 63-75 (held in Phoenix, AZ, 14 November 1982).

Sines, G. H., Z. Yang, and B. D. Vickers, Effect of the Matrix on the Creep-Behavior of Carbon-Carbon Composite, UCLA School of Engineering Report UCLA-ENG-87-44 (November 1987).

White, J. L., "Formation of Microstructure in Graphitizable Materials," in Progress in Solid State Chemistry, Vol. 10, ed. H. Reiss (Pergamon, New York, 1977), pp. 59-104.

Zimmer, J. and R. Wietz, 17th Biennial Carbon Conference (American Carbon Society, 1985), pp. 396-397 (held at University of Kentucky, Lexington, 16-21 July 1985).

Zukas, E. G. and W. V. Green, "Creep Behavior of Hot Isostatically Pressed Graphite," 9th Biennial Conference on Carbon, pp. 69-70 (held at Boston College, Boston, MA, 16-20 June 1969).

APPENDIX: MODULUS CALCULATIONS

A.1. SAMPLE CALCULATION OF MODULUS TRANSLATION EFFICIENCY

A sample calculation of modulus translation efficiency is given below. For a P55/A240 composite sample (see Table 3), the measured modulus, E, was 22.7 Msi and average sample diameter, D, was 0.78 mm. The yarn area, A_1, is given by

$$A_1 = \frac{\pi N D^2}{4} = 4.8 \times 10^{-3} \text{ cm}^2 \qquad \text{(A-1)}$$

where N = 2000 filaments and D = 10 μm for P55 fiber. The sample cross-sectional area, A_2, is calculated from the average sample diameter, assuming a circular cross section:

$$A_2 = \frac{\pi D^2}{4} = 4.8 \times 10^{-3} \text{ cm}^2 \qquad \text{(A-2)}$$

where D = 0.78 mm.

The fiber volume fraction is obtained from the ratio of yarn area to sample area,

$$N_f = \frac{A_1}{A_2} = 32.9\% \qquad \text{(A-3)}$$

The ROM modulus value is

$$E_{ROM} = E_f V_f = 18 \text{ Msi} \qquad \text{(A-4)}$$

where E_f = 55 Msi for P55 fiber. Note that this value is less than the measured modulus.

A.2. SAMPLE CALCULATION OF EFFECTIVE MATRIX MODULUS

In the example described above, the measured modulus value exceeded the calculated ROM value. An effective matrix modulus can be calculated from density measurements and assuming good fiber-matrix bonding and stress transfer through the matrix. The porosity, V_p, is estimated from the bulk density, ρ_b (total mass/total volume, including pores), 1.26 g/cm^3, and the true density, ρ_a, 1.8 g/cm^3, measured by immersion in a methanol and dibromoethane mixture:

$$V_p = 1 - \frac{\rho_b}{\rho_a} = 30\% \qquad \text{(A-5)}$$

The matrix volume fraction, V_m, is estimated from

$$1 = V_f + V_m + V_p \qquad \text{(A-6)}$$

which gives $V_m = 37.1\%$. Finally, we obtain an apparent matrix modulus, E_m, from the rule of mixtures:

$$E_{measured} = E_f V_f + E_m V_m \qquad \text{(A-7)}$$

Solving for E_m, we obtain $E_m = 12$ Msi. As discussed in the text, this large value suggests the presence of a sheath of material with preferred orientation surrounding the fiber.

The values used for other carbon yarns were as follows: for HM 3000, N = 3000, D = 7 μm, and E = 50 Msi; and for WCA, N = 1440 and D = 9 μm. A value for E was not obtained for the WCA cloth because of yarn crimping.